An Electro-Optic Pulsed NVNA Load-Pull System for Distributed E-field Measurements

Jonas Urbonas, *Student Member, IEEE,* Kevin Kim, *Member, IEEE,* Frederik Vanaverbeke and Peter H. Aaen, *Senior Member, IEEE*

***Abstract*—In this paper, a new combined electro-optic and pulsed nonlinear vector network analyser-based load-pull measurement system for distributed multi-harmonic electric field measurements is presented. The system uses an external electro-optic probe to measure cross-frequency phase-coherent multi-harmonic vector E-fields with an 8 µm spatial resolution and 20 MHz – 20 GHz bandwidth. We demonstrate the performance of the distributed phase-coherent E-field measurements of E_x, E_y and E_z components with 3 harmonics above a commercially available large periphery, packaged, laterally diffused metal-oxide-semiconductor (LDMOS) transistor. The transistor was measured at 2.2 GHz under pulsed conditions with 10 µs pulse and 10 % duty cycle, while outputting 55.1 dBm of power. The measured electric fields of the operating transistor are animated for the first time and reveal complex non-uniform operation at harmonic frequencies.**

***Index Terms*—Device characterization, electro-optic sampling, laterally diffused metal-oxide-semiconductor (LDMOS) transistor, load-pull, near-field measurement**

I. Introduction

THE large periphery power amplifiers often contain multiple transistor dies and can suffer from non-uniform distributions of current and voltage across the die, resulting in increased power dissipation, degraded device efficiency and output power [1], [2]. This poses a challenge when such circuits need to be analysed during device prototyping, as conventional measurement techniques treat the device under test (DUT) as a black box, i.e., only the input and output port-based response of the device is measured providing traditional metrics like gain, efficiency etc., with no indication of the internal device operation. While real-time de-embedding methods in conjunction with active load-pull (LP) allow inspection of the intrinsic drain current and voltage, without the readily-available distributed packaged transistor models they are still just the port based measurements providing no information of the internal distributed device operation [3]. The distributed device behaviour has been addressed in the simulation domain by the introduction of multiphysics-based modelling approaches [1], [4]. The direct validation of these models is very challenging for low power devices or not accessible for high power devices with complex matching networks.

Measuring the electromagnetic fields above packaged high-power transistors provides new information and has become a new area of exploration in the microwave design community [2], [5], [6]. To measure distributed device behaviour various contactless probing techniques have been developed and they can be divided into two main categories: metallic and dielectric. Most of the metallic probes are based on a cut coaxial probe geometry [2], [5], [7] acting as a monopole antenna, although small dipole-based [8] and active electric field (E-field) probes [6] have also been developed. Metallic probes are very inexpensive to produce and exhibit high E-field sensitivity, but can suffer from probe invasiveness as they modify the fields above the DUT.

Dielectric probes are virtually non-invasive and thus only minimally perturb the E-fields above the DUT. There are two main dielectric probing techniques: quantum-based probes and electro-optic probes. Quantum based probes [9], which are still very much in their initial research and have yet to be miniaturised, are not yet suited for the distributed device behaviour characterisation. Moreover, quantum based probes are sensitive to the full E-field, and cannot measure the E-field vector components independently. Electro-optic (EO) E-field measurement techniques are very well suited for distributed field characterization as they have very high spatial resolutions, are minimally invasive, and can measure all vector components of the E-field.

The electro-optic measurement technique is based on a linear electro-optic effect, whereby an electric field dynamically changes the birefringence properties of an anisotropic crystal, which in turn changes the polarisation of light passing through it. If the crystal is placed between two cross-polarisers, it can be used as a laser light retarder that induces a change in the light intensity which is directly proportional to the polarisation change [10]. The spatial resolution of the measurement technique is dependent on the laser beam spot size which can be as small as 0.5 µm [11]. The use of ultra-fast lasers combined with the temporal resolution of EO crystals allow measurements up to THz frequencies [12] using both internal [13]–[15] and external [16], [17] electro-optic sampling (EOS) techniques. The internal EOS technique relies upon the device substrate acting as a birefringent material limiting its applicability to a narrow range of semiconductors, and excludes it from packaged device measurements.

The external EO probing technique uses EO crystals placed

Manuscript received March 7, 2018; accepted XXXXX XX, 2017. Date of publication Month XX, XXXX. This work was funded and supported by NXP semiconductor and the EPSRC grant EP/L02263X/1.

J. Urbonas and P. H. Aaen are with the Department of Electrical and Electronic Engineering, Advanced Technology Institute, n3m-labs, University of Surrey, Guildford, Surrey, GU2 7XH, United Kingdom, e-mail: j.urbonas@surrey.ac.uk. K. Kim and F. Vanaverbeke are with the RF Power Division, NXP Semiconductors, Chandler, AZ, United States.

Colour version of one or more of the figures in this paper are available online at http://ieeexplore.ieee.org

Digital Object Identifier XX.XXXX/LMWC.XXXX.XXXXXXX

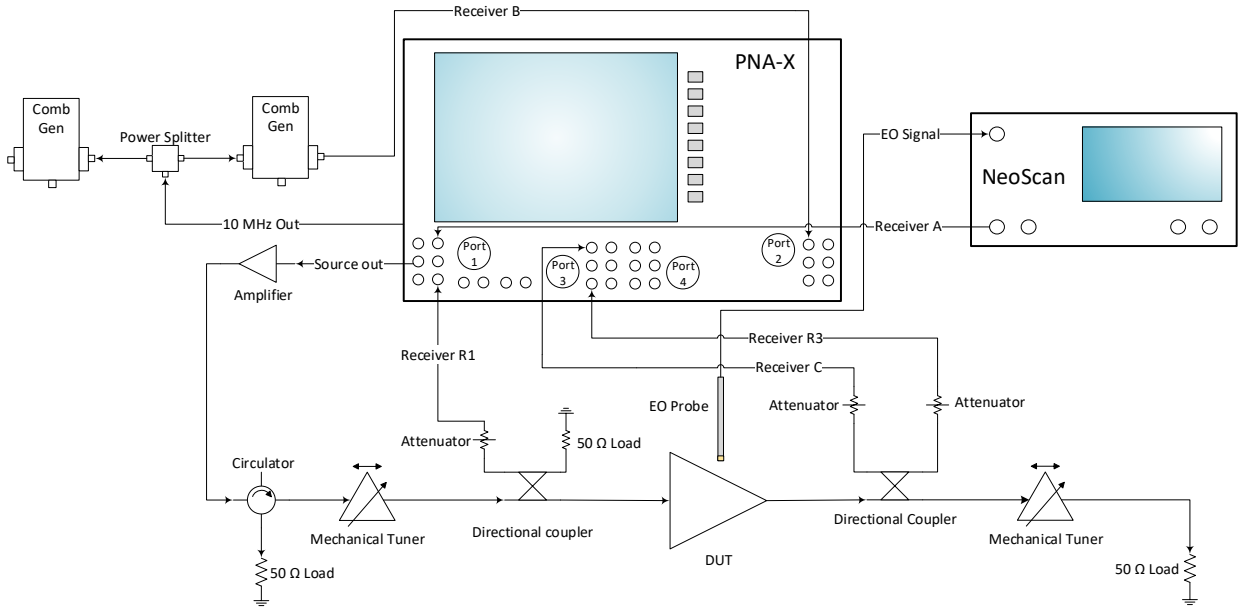

Fig. 1. Schematic showing an integrated electro-optic and pulsed NVNA load-pull measurement system for non-invasive multi-harmonic vector E-field measurements combining commercially available EO and NVNA measurement systems. The source- and load-pull are enabled by two slide-screw mechanical tuners with the bandwidth of 0.8 – 18 GHz.

in the vicinity of the DUT, that allow the E-field to be measured anywhere around the DUT regardless of its geometry or substrate material. Since the crystal birefringence is sensitive only to a single E-field component, the external EO technique can separately measure all three (E_x, E_y, E_z) E-field components. Although the crystal is placed in the vicinity of the DUT, the invasiveness of the probe is virtually nonexistent due to its dielectric nature [18]–[22] and no signal is coupled away, unlike in the case of the metallic probes.

When characterising a high-power microwave PA, measurement of large signal data is imperative to fully capture the non-linear behaviour, and load-pull measurements are often performed. To reconstruct the large signal time-domain (TD) waveforms at the device reference planes cross-frequency phase coherence is needed. Thus, a non-linear vector network analyser (NVNA) combined with a load-pull measurement system is used [23].

The cross-frequency phase coherence is established by using an external phase reference, which is used to correct the phase of the measured harmonics,

$$\Phi_n^{corr} = \Phi_n^{meas} - (\Phi_n^{rm} - \Phi_n^{rc}) \quad (1)$$

where Φ_n^{meas} is the measured phase, Φ_n^{rm} is the measured phase of the reference, Φ_n^{rc} is the pre-characterised phase of the reference, n is the number of the harmonic being measured, and Φ_n^{corr} is the phase correction factor [24].

In this paper, a new, combined electro-optic and pulsed NVNA LP measurement system is presented that enables distributed time-domain vector E-field measurements under continuous wave (CW) or pulsed operation. Section II presents the measurement set-up used to measure the distributed device behaviour, Section III discusses the system calibration and verification using a microstrip measurement, and Section IV presents multi-harmonic phase-coherent E-field vector measurements of a 260-W LDMOS transistor measured under pulsed RF conditions. The reconstruction of time-domain E-fields from the measured multi-harmonic fields is demonstrated and insights into the operation of the packaged transistor, and the potential for design improvements are suggested. Finally, Section V concludes the paper.

II. Measurement Set-up

The measurement set-up, as shown in Figs. 1 and 2 uses a commercially available NeoScan® EO measurement system manufactured by EMAG Technologies Inc.[1], which uses an external optical-fibre-coupled $Bi_{12}SiO_{20}$ (BSO) crystal-based probes for vector E-field measurements. The system has an 8 µm spatial resolution and is able to measure E-field vector components (E_x, E_y and E_z) over a 20 MHz – 20 GHz bandwidth. The probe is designed to measure fields from 1 V/m to 2 MV/m; other smaller [25] and more sensitive probes have also been designed [26].

The standard system configuration uses a lock-in amplifier for single frequency E-field measurement. A photonic down-conversion technique is utilised to increase the measurement sensitivity and detect the phase of the measured signal, as all of the equipment is working in a phase-locked loop configuration [27]. The use of lock-in amplifiers is not suited for pulsed signal measurements as they are measuring the root-mean-square of the voltage, while high-power microwave PAs are often operated under pulsed conditions. Moreover, the lock-in approach does not allow multi-harmonic measurements with cross-frequency phase coherence. The optical mainframe, which is part of the standard EO system configuration, outputs a measured time domain signal, but the lock-in amplifier locks only on a single frequency component of that signal.

[1] www.emagtech.com

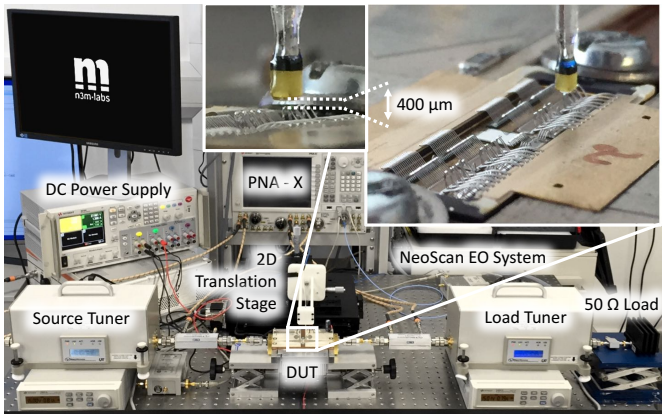

Fig. 2. Fully assembled electro-optic and pulsed NVNA load-pull measurement system. During the E-field scan, the probe was positioned 400 µm above the tallest bondwires of the DUT.

If the lock-in frequency is changed to measure a harmonic of the fundamental frequency, the phase reference of the signal is lost, thus the reconstruction of the time-domain signal becomes impossible. Also, real-time measurements using an oscilloscope are impractical for distributed time-domain E-field measurements due to the high thermal noise of the EO system, low measurement sensitivity, and a large number of coherent averages required. To overcome this, the NeoScan optical mainframe is connected to Keysight N5247A PNA-X 67 GHz microwave vector network analyser. Using the NVNA with a comb generator (U9391G) as a reference for cross-frequency phase coherence instead of the lock-in amplifier allows an accurate reconstruction of the TD signal measured by the electro-optic system.

The source- and load-pull are performed by using two Maury mechanical impedance tuners (MT982BL01) with 0.8 – 18 GHz bandwidth and 0.5 kW peak power handling capability. The tuners and the load-pull measurements are controlled by IVCAD^{TM} measurement software. Since the system has a coupler connected for the measurement of "*a*" and "*b*" waves either on the input or on the output of the DUT, it is possible to use this set-up for either source- or load-pull measurements and to measure the multi-harmonic E-fields above the transistor for any source or load impedance. Source-pull measurements are enabled by connecting the receiver A of the PNA-X to the input directional coupler, and connecting the output of the EO system to receiver C. Moreover, the same set-up can be used for active load-pull measurements by removing the tuners from the set-up in Fig. 1 and using another amplifier for active signal injection at the output side of the DUT. Although the PNA-X is a 4-port analyser, only the receivers on ports 1 and 3 can be used for the measurements, as the NVNA measurement mode is software-restricted by the manufacturer to these ports.

During measurement, the EO probe is placed into an all-dielectric holder that is mounted on a 2D translation stage, as shown in Fig. 2. The translation stage is then moved by fixed steps within the x-y plane to enable the EO probe to measure the E-fields above the DUT. The measurement is controlled by a custom LabVIEW^{TM}-based control software, which triggers the pulsed NVNA measurements and synchronously controls the movement of the 2D translation stage. The fully assembled measurement system is shown in Fig. 2. This set-up allows fully automated measurements of the distributed multi-harmonic E-fields with cross-frequency phase coherence under different source and load impedances.

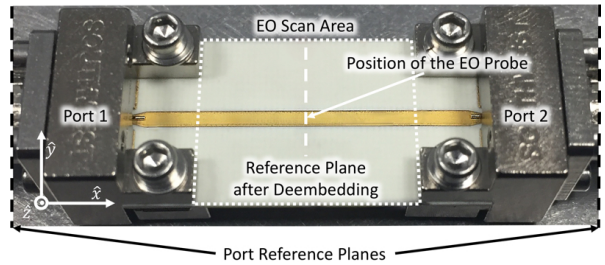

Fig. 3. Photograph of the microstrip used for system verification and time-domain waveform calibration.

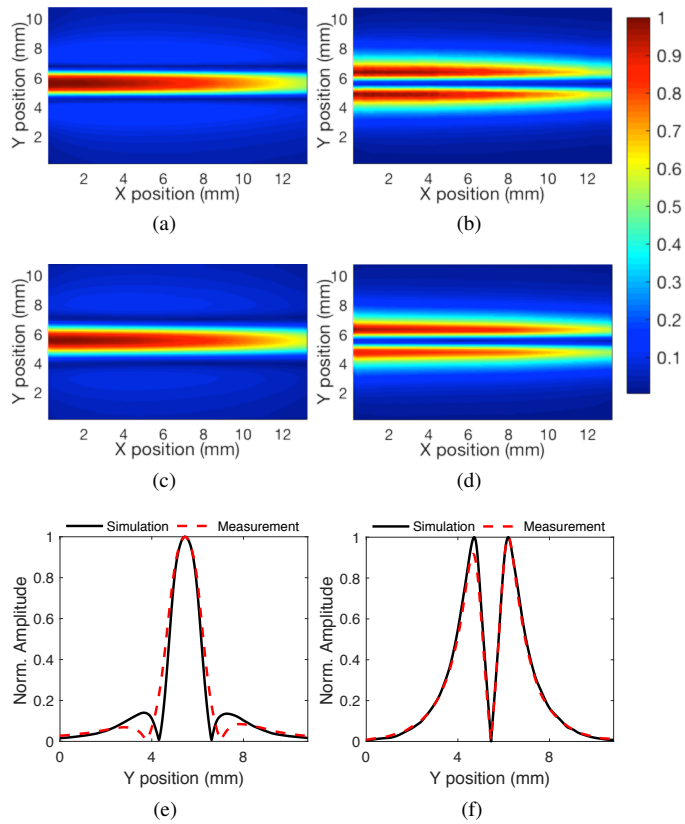

Fig. 4. Simulated (a), (b) and measured (c), (d) normalised E_z (a), (c), (e) and E_y (b), (d), (f) E-field distributions along the microstrip transmission line. A comparison between the simulation and measurement is also shown in cut-line E-field distributions along the *y*-axis (e), (f).

III. System Verification and Calibration

The verification of the system to measure the E-field distribution and time-domain waveforms is a three step process. Firstly, a microstrip transmission line, shown in Fig. 3, was simulated in a finite-element-based electromagnetic (EM) simulator EMPro^{TM}, and measured under pulsed conditions providing the distributed E-fields. Secondly, a time-domain signal above the microstrip is measured and a calibration factor

is derived by comparing it to the NVNA port reading, enabling the measurement of absolute time-domain waveforms. Finally, the calibrated system is used to measure a different time-domain signal verifying the measurement of the distributed E-fields and time-domain waveforms.

To obtain the distributed E-field measurements shown in Fig. 4, a pulsed signal was used to excite the microstrip, which had a 10 µs pulse width, 100 µs period and P_{in} = 40 dBm, similar to the input power to be used with PA. The 17.8 µm thick gold microstrip was fabricated on a 508 µm Rogers RO4350 substrate. Southwest Microwave sma-to-microstrip end launch connectors were used to access the microstrip. Both E_y and E_z components of the E-field were measured at 2.2 GHz and compared to the simulation. The E-field scan was performed along the y-axis. The translation stage step size was 200 µm, and the EO probe was positioned 250 µm above the DUT. The measurement and simulation show a very good E-field agreement.

During the time-domain measurements, the NVNA uses an external phase reference for cross-frequency phase coherence. The relative harmonic phases are automatically obtained [24], which enables the time-domain E-field reconstruction at all measurement points above the DUT. The TD E-field reconstruction from the measured data is computed by,

$$E_{TD} = \sum_{n=1}^{k} \mathrm{Re}\{\kappa_n E_n e^{jn\omega t}\} \tag{2}$$

where E_{TD} is the time-domain distributed electric field above the DUT, κ is the correction factor defined in (4) , ω is the radial frequency, t is time, n is the harmonic number, k is the number of measured harmonics and E_n is the measured electric field at nth harmonic as given by

$$E_n = \begin{bmatrix} E_{n_{0,0}} & E_{n_{1,0}} & \dots & E_{n_{x,0}} \\ E_{n_{0,1}} & \dots & \dots & \dots \\ \dots & \dots & \dots & \dots \\ E_{n_{0,y}} & \dots & \dots & E_{n_{x,y}} \end{bmatrix} \tag{3}$$

where x and y are the translation stage coordinates of x- and y-axes respectively.

The amplitude and phase of the raw EO signal measured at the NVNA receiver is calibrated by comparing it to the measurement obtained at the NVNA ports [28]. To achieve this, a microstrip from Fig. 3 is used. Firstly, the NVNA is calibrated using a short-open-load-thru (SOLT) vector receiver calibration, an absolute phase calibration using a comb generator, and an absolute power calibration using a power meter up to the port reference planes. Then two S-parameter files for each half of the fixture, obtained using a thru-reflect-line (TRL) calibration, are used to move the port reference planes up to the middle of the microstrip as shown in Fig. 3. A pulsed time-domain waveform, generated by biasing an ATF-54143 gallium arsenide (GaAs) pseudomorphic high electron mobility transistor (pHEMT) in deep class C operation, is then injected at port 1 and measured by the NVNA. The PNA-X was configured to measure 3 harmonics of a 2.2 GHz fundamental. The noise bandwidth was set to 500 Hz and the averaging was set to 10.

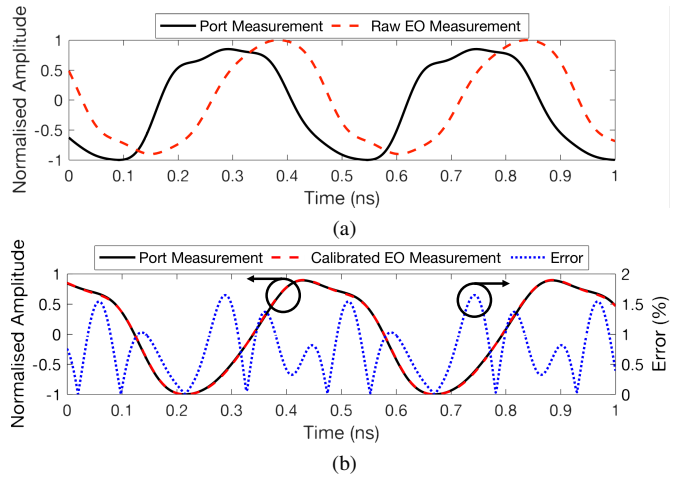

Fig. 5. Time-domain waveform used to obtain the correction factor (a), and a calibrated waveform of a different device using the same correction factor (b). Both waveforms are reconstructed using 5 harmonics.

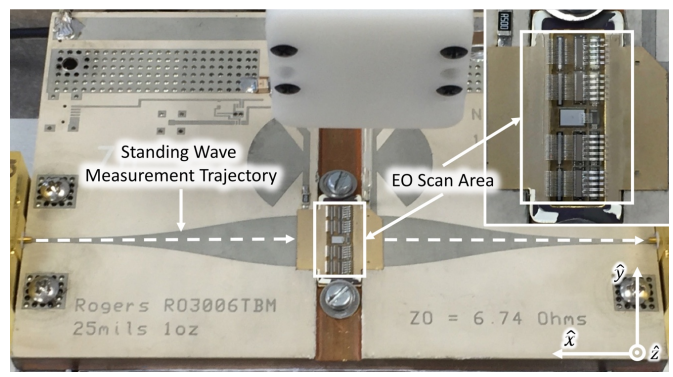

Fig. 6. Transistor fixture image showing the E-field scan axes, EO scan area (12 mm x 18 mm) on the zoomed-in image of the LDMOS transistor, and the scan trajectory used for standing wave measurements from Fig. 8 along the impedance transformer.

After the NVNA measurement is obtained, the NVNA calibration is turned off, and the receiver A is connected to the EO system. The EO probe was positioned 50 µm above the line in the middle of the microstrip as indicated in Fig. 3. The same time-domain signal is then injected at port 1, and the raw EO signal measurement is obtained as shown in Fig. 5(a). Because a pre-amplifier is used in the optical mainframe of the EO system, the TD waveform is inverted and has a frequency dependent amplitude. The NVNA receivers might also exhibit frequency dependency, thus the amplitude calibration at all harmonics is important to correctly recreate the TD waveform. Furthermore, there is a phase shift associated with the internal circuitry of the EO system and cables connecting it to the NVNA, thus the phase correction also needs to be applied. The correction factor can then be defined as

$$\kappa_n = \frac{|b_{2_n}^{norm}|}{|EO_n^{norm}|} e^{jn(b_{2_{fund}} - EO_{fund})} \tag{4}$$

where $|b_{2_n}^{norm}|$ is the normalised magnitude of the b_2 wave, $|EO_n^{norm}|$ is the normalised magnitude of the EO signal, n is the harmonic number, $b_{2_{fund}}$ is the phase angle in radians of the b_2 wave at the fundamental frequency, and EO_{fund} is

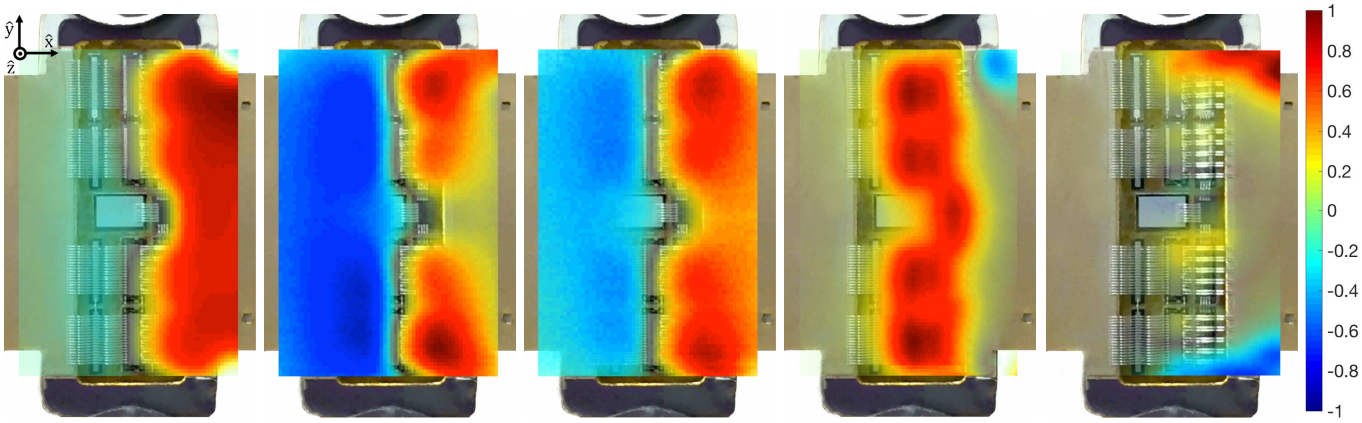

(a) (b) (c) (d) (e)

Fig. 7. Measured normalised E-field components overlaid on images of the transistor showing the E_z component for 2.2 GHz fundamental, 2nd and 3rd harmonics in (a), (b), and (c) respectively, a full time-domain reconstructed (using 3 harmonics) E_x component (d) and a full time-domain E_y component (e). The gate of the transistor is located on the left hand side of the package with the drain on the right and the normalised E-field distributions are shown at their peak amplitudes. Animations are provided for all configurations showing the time varying fields in movies Fig_7a-e.mov.

the phase angle in radians of the inverted EO signal at the fundamental frequency.

After the correction factor is obtained, it can be used to correct any EO signal for absolute waveform measurements. The verification of this approach is illustrated in Fig. 5(b) where the NVNA signal measurement at the centre of the microstrip is compared to the calibrated EO signal. The new TD waveform is generated by driving a Minicircuits ZRL-2400LN amplifier into compression at 2.2 GHz (P_{in} = 10 dBm, P_{out} = 26 dBm). The correction factor for this measurement was obtained from the waves in Fig. 5(a), and since the probe is virtually non-invasive, the waveforms show almost a perfect agreement with a 1.64% max error.

IV. LDMOS Measurement Results

The measured device was a commercially available A2T21S260W12N LDMOS transistor that has 4 LDMOS dies, metal oxide-semiconductor (MOS) capacitors, interconnected with over 100 bondwires forming matching networks all housed in an air-cavity metal ceramic package. The pre-matching network is a T-network composed of arrays of bondwires and a MOS capacitor and the post-match is a shunt-L configuration. In addition, circuitry to improve the video bandwidth of the packaged transistor is placed between pairs of die along the centre axis of the transistor at the output. The transistor package lid was removed for all of the measurements.

Firstly, pulsed NVNA LP measurements were performed using the vector-receiver load-pull set-up. The load impedance presented to the DUT was controlled at the fundamental frequency to find the maximum output power impedance. The transistor was driven by a 40-W Amplifier Research pre-amplifier (40S1G4). To maximise the input power, the source tuner reflection coefficient was conjugately matched to the input reflection coefficient of the DUT. The measurement reference planes were at the 3.5 mm connectors of the load-pull test fixture. The LDMOS transistor was biased at V_{ds} = 28 V, I_{ds} = 1.48 A, V_{gs} = 2.64 V, and RF input was a pulsed continuous wave with 10 µs pulses, and a 10 % duty cycle.

After the maximum power, at the 3-dB gain compression point (P_{3dB}), load impedance was identified, the EO system was connected to receiver A of the PNA-X. The same impedances were used during the distributed multi-harmonic E-field measurements. The input power, P_{in}, was set to 42.5 dBm resulting in P_{out} of 55.1 dBm. The EO probe was positioned 400 µm above the tallest bondwires of the DUT as shown in Fig. 2. To achieve high resolution measurements, long duration scans were performed. During the scans the total power of the output and reflected laser beams were monitored to ensure measurement stability. A thermo-electric cooler was used to prevent any polarisation drift in the laser beam [29]. The DUT scan area was 12 mm x 18 mm, as shown in Fig. 6, and the translation stage step size was 100 µm on x- and 200 µm on y-axes for E_x, 200 µm on x- and 100 µm on y-axes for E_y and 200 µm on both x- and y-axes for E_z field measurements. The scan time was 4 hours for the E_z component with 3 harmonics (5551 points), and 8 hours for both E_x (11011 points) and E_y (11041 points). The PNA-X measurement configuration was the same as indicated in Section III. In this paper, the relative distributed E-field results are normalised to their own maximum. This is valid as the E-field and light polarisation change relationship inside the EO crystal is scalar and linear. Thus the absolute E-field amplitude calibration is not necessary, albeit possible by employing micro transverse electromagnetic (µ-TEM) cells that allow the determination of the scalar E-field amplitude calibration factor [30]–[32].

All three harmonics of the E_z field component are presented in Fig. 7 along with the full time-domain-reconstructed E_x and E_y components. The measured E_z field distribution across the transistor is fairly uniform at the fundamental frequency as can be seen in Fig. 7a, but the 2nd and 3rd harmonics in Fig. 7b and Fig. 7c respectively are showing a non-uniform E-field distribution. This suggests that the DUT is well optimised at the fundamental frequency, but the harmonic terminations for all individual fingers might not be optimal. The E_x field measure-

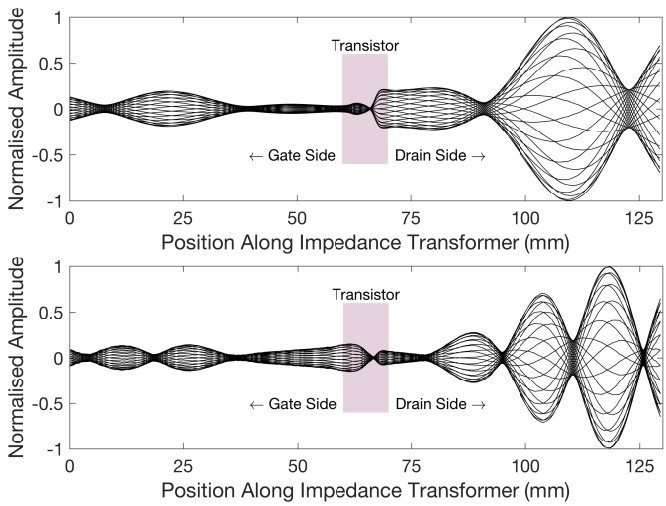

Fig. 8. Standing wave E_z measurements along the transistor fixture as shown in Fig. 6 of the 2.2 GHz fundamental (top) and 2nd harmonic (bottom). The standing wave at the fundamental frequency results in a local maximum on the drain side of the DUT, whereas the 2nd harmonic results in a minimum.

ments are showing a strong drain-to-gate coupling as shown in Fig. 7d, as a consequence of the gate-to-drain (C_{gd}) capacitance of the packaged transistor. The E_y (Fig. 7e) field component, on the other hand, is showing minimal coupling between the transistor dies as they all operate at the same potential.

As can be seen from the E-field plots in Fig. 7, the fundamental (a) and the 3rd harmonic (c) of the E_z component are showing a typical amplifier behaviour, whereby the input signal on the gate side of the DUT is amplified on the drain side. The 2nd harmonic (b) is showing the opposite behaviour with gate-side having a larger amplitude signal, than the drain side. This is due to the EO probe measuring the full E-field rather than just the forward and backward travelling waves. The combination of both waves forms a standing wave along the impedance transformer of the transistor fixture. This is shown in Fig. 8 for the case of the fundamental and the 2nd harmonic. The 2nd and 3rd harmonics on the gate side of the packaged transistor are produced by the pre-amplifier used in the set-up that is operating at its maximum gain setting and the drain-to-gate signal coupling of the DUT.

To further the examination of the performance of the packaged transistor the normal component of the electric field, E_z, was extracted across all drain bondwires where the electric field is at its most intense. The normalized fields of the fundamental and second harmonic at two different impedance points are plotted over one period to show variation of the electric field above the bondwires with time, as shown in Fig. 9. The first is the P_{3dB} impedance point, and the other one is P_{3dB} with a phase shift of 60°. The input power to the DUT was 42.5 dBm at both impedance points. Changing the impedance also decreased the P_{out} value by 7 dB at 2.2 GHz for the same gain compression. The E-fields at 2.2GHz, across all four arrays of bondwires, remain almost constant in both cases, with fields above the inner most wires being slightly lower than those towards the outside of the package. While at the second harmonic, 4.4 GHz, there is a significant variation as fields above the bondwire arrays connected to the

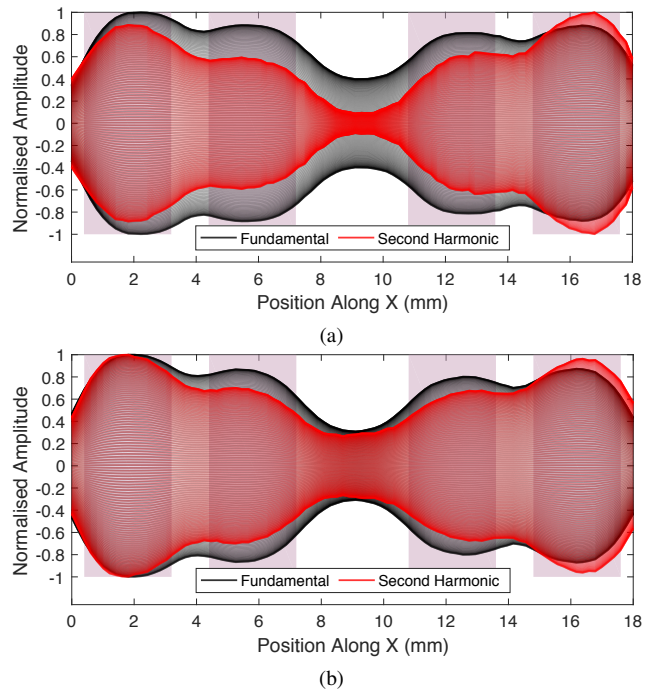

Fig. 9. Normalised amplitude plots of the fundamental and second harmonics of the E_z electric field component along the top of the drain wires at a max P_{out} impedance point (a) and a sub-optimal point (b). The shaded areas indicate approximate positions of the drain bondwires within the package.

two internal dies only reach 60%-70% of the maximum value of the bondwire arrays connected to the two external dies.

The variation of the field at the second harmonic is very significant and designers optimize their matching network design so that all dies are performing optimally. Despite each die and its associated matching network being identical, within manufacturing tolerances, the second harmonic E-field components are non-uniform in both Fig. 9a and 9b with Fig. 9a exhibiting stronger non-uniformity. While this is true for the 2nd harmonic, the E-field distribution at the fundamental frequency for the same impedance point is more uniform than the one in Fig. 9b. This, together with an 8 dB lower amplitude of the 2nd harmonic generated by the transistor leads to a better device performance and higher output power at the P_{3dB} impedance point. It also suggests that the harmonic impedances presented to the two internal transistors could be improved to further increase the efficiency of the packaged transistor.

While the measurement time for detailed scanning and animation over the entire packaged transistor can be quite long, the measurement of a single cut, as shown in Fig. 9, only takes approximately 4 minutes suggesting that it can be used in a commercial laboratory setting to aid in the design and optimization of microwave power amplifiers.

V. Conclusions

A combined EOS and NVNA based load-pull measurement system for minimally invasive multi-harmonic E-field measurements is presented. The system functionality is demonstrated by the measurement of the distributed phase-coherent E-fields with all three vector components (*x, y, z*) above a 260-W large periphery packaged LDMOS transistor operating at 2.2 GHz. The measured E-fields are animated and visualised

showing a time-domain wave in the transistor operating at 55.1 dBm output power. This technique presents a new method to visualise and hence understand the complex dynamics that occur in the complex package devices.

Acknowledgment

The authors would like to thank Prof. Nick Ridler for valuable metrology discussions.

References

[1] P. H. Aaen *et al.*, "Multiphysics Modeling of RF and Microwave High-Power Transistors," *IEEE Trans. Microw. Theory Techn.*, vol. 60, no. 12, pp. 4013–4023, Nov. 2012.

[2] H. Rui *et al.*, "Non-intrusive Near-field Characterization of Distributed Effects in Large-periphery LDMOS RF Power Transistors," in *IEEE MTT-S Int. Microw. Symp. (IMS)*, Pheonix, AZ, USA, 2015, pp. 1–3.

[3] F. Vanaverbeke *et al.*, "Real-time non-linear de-embedding," in *77th Microw. Meas. Conf. (ARFTG)*, Baltimore, MD, USA, 2011, pp. 1–6.

[4] D. Denis, C. M. Snowden, and I. C. Hunter, "Coupled Electrothermal, Electromagnetic, and Physical Modeling of Microwave Power FETs," *IEEE Trans. Microw. Theory Techn.*, vol. 54, no. 6, pp. 2465–2470, Jun. 2006.

[5] R. Hou *et al.*, "Nonintrusive Near-Field Characterization of Spatially Distributed Effects in Large-Periphery High-Power GaN HEMTs," *IEEE Trans. Microw. Theory Techn.*, vol. 64, no. 11, pp. 4048–4062, Oct. 2016.

[6] N. Dehghan *et al.*, "An Improved Electric Field Probe with Applications in High Efficiency PA Design and Diagnostics," in *81st Microw. Meas. Conf. (ARFTG)*, Seattle, WA, USA, 2013, pp. 1–4.

[7] L. Nativel *et al.*, "MMIC's Characterization by Very Near-field Technique," *Microw. Opt. Technol. Lett.*, vol. 41, no. 3, pp. 209–213, Mar. 2004.

[8] T. P. Budka, S. D. Waclawik, and G. M. Rebeiz, "A Coaxial 0.5-18 GHz Near Electric Field Measurement System for Planar Microwave Circuits Using Integrated Probes," *IEEE Trans. Microw. Theory Techn.*, vol. 44, no. 12, pp. 2174–2184, Dec. 1996.

[9] C. L. Holloway *et al.*, "Broadband Rydberg Atom-Based Electric-Field Probe for SI-Traceable, Self-Calibrated Measurements," *IEEE Trans. Antennas Propag.*, vol. 62, no. 12, pp. 6169–6182, Sep. 2014.

[10] M. S. Heutmaker *et al.*, "Electrooptic Sampling of a Packaged High-Speed GaAs Integrated Circuit," *IEEE J. Quantum Electron.*, vol. 24, no. 2, pp. 226–233, Feb. 1988.

[11] G. David *et al.*, "Electro-optic probing of RF signals in submicrometre MMIC devices," *Electron. Lett.*, vol. 31, no. 25, pp. 2188–2189, Dec. 1995.

[12] J. Valdmanis and G. Mourou, "Subpicosecond Electrooptic Sampling: Principles and Applications," *IEEE J. Quantum Electron.*, vol. 22, no. 1, pp. 69–78, Jan. 1986.

[13] D. R. Hjelme, M. J. Yadlowsky, and A. R. Mickelson, "Two-Dimensional Mapping of the Microwave Potential on MMICs Using Electrooptic Sampling," *IEEE Trans. Microw. Theory Techn.*, vol. 41, no. 6, pp. 1149–1158, Jun./Jul. 1993.

[14] G. David *et al.*, "Two-dimensional direct electro-optic field mapping in a monolithic integrated GaAs amplifier," in *23rd Eur. Microw. Conf.*, Palacio de Congresos, Madrid, Spain, 1993, pp. 497–499.

[15] ——, "In-circuit Electro-Optic Field Mapping for Function Test and Characterization of MMICs," in *IEEE MTT-S Int. Microw. Symp. Dig.*, vol. 3, San Francisco, CA, USA, 1996, pp. 1533–1536 vol.3.

[16] D.-J. Lee *et al.*, "Recent Advances in the Design of Electro-Optic Sensors for Minimally Destructive Microwave Field Probing," *Sensors*, vol. 11, no. 1, p. 806, Jan. 2011.

[17] C. T. Rodenbeck *et al.*, "Electrooptic Inspection of Vector Leakage in Radiofrequency Multichip Modules," *IEEE Trans. Electromagn. Compat.*, vol. 55, no. 6, pp. 1093–1099, Jul. 2013.

[18] H. J. Cheng *et al.*, "Electro-Optic Probes: High-Permittivity Crystals vs. Low-Permittivity Polymers," in *Ultrafast Electron. and Optoelectron.*, ser. OSA Tech. Dig. Series. Dana Point, CA, USA: Optical Society of America, 1995, p. UTUE1 vol.13.

[19] W. Mertin *et al.*, "Probe Tip Invasiveness at Indirect Electro-Optic Sampling of MMIC," in *IEEE MTT-S Int. Microw. Symp. Dig.*, Atlanta, GA, USA, 1993, pp. 1351–1354 vol.3.

[20] D. J. Lee and J. F. Whitaker, "An optical-fiber-scale electro-optic probe for minimally invasive high-frequency field sensing," *Opt. Express*, vol. 16, no. 26, pp. 21 587–21 597, Dec. 2008.

[21] S. Seitz *et al.*, "Characterization of an external electro-optic sampling probe: Influence of probe height on distortion of measured voltage pulses," *J. Appl. Phys.*, vol. 100, no. 11, p. 113124, Dec. 2006.

[22] D. J. Lee, J. Y. Kwon, and N. W. Kang, "Field analysis of electro-optic probes for minimally invasive microwave sampling," *Opt. Express*, vol. 22, no. 3, pp. 2897–909, Jan. 2014.

[23] D. Barataud, M. Campovecchio, and J. M. Nebus, "Optimum design of very high-efficiency microwave power amplifiers based on time-domain harmonic load-pull measurements," *IEEE Trans. Microw. Theory Techn.*, vol. 49, no. 6, pp. 1107–1112, Jun. 2001.

[24] D. E. Root *et al.*, *X-Parameters*. Cambridge University Press, 2013.

[25] D. J. Lee and J. F. Whitaker, "A simplified fabryperot electro-optic modulation sensor," *IEEE Photon. Technol. Lett.*, vol. 20, no. 10, pp. 866–868, Apr. 2008.

[26] K. Sasagawa and M. Tsuchiya, "An electrooptic sensor with sub-millivolt sensitivity using a nonlinear optical disk resonator," in *Int. Topical Meeting Microw. Photonics (MWP)*, Seoul, Korea, 2005, pp. 355–358.

[27] K. Sasagawa, M. Tsuchiya, and M. Izutsu, "Sensitivity Enhancement of Electrooptic Probing Based on Photonic Downconversion by Sideband Management," in *Quant. Electron. Laser Sci. Conf. (QELS)*, ser. Tech. Dig. (CD). Baltimore, MD, USA: Optical Society of America, 2005, p. JWB5.

[28] R. Hou *et al.*, "Contactless Measurement of Absolute Voltage Waveforms by a Passive Electric-Field Probe," *IEEE Microwave Wireless Compon. Lett.*, vol. 26, no. 12, pp. 1008–1010, Nov. 2016.

[29] A. A. Aly and A. S. A. El-Lail, "Fuzzy Temperature Control of A Thermoelectric Cooler," in *IEEE Int. Conf. Ind. Technol.*, Mumbai, India, 2006, Conference Proceedings, pp. 1580–1585.

[30] D. J. Lee *et al.*, "Calibrated 100-dB-dynamic-range electro-optic probe for high-power microwave applications," *Opt. Express*, vol. 19, no. 15, pp. 14 437–14 450, Jul. 2011.

[31] N. W. Kang *et al.*, "Characterization Method of Electric Field Probe by Using Transfer Standard in GTEM Cell," *IEEE Trans. Instrum. Meas.*, vol. 58, no. 4, pp. 1109–1113, Dec. 2008.

[32] D.-J. Lee *et al.*, "Field-calibrated electro-optic probe using interferometric modulations," *J. Opt. Soc. Am. (JOSA) B*, vol. 27, no. 2, pp. 318–322, Jan. 2010.

Jonas Urbonas received the B.Eng degree in Electronic Engineering from the University of Surrey, Guildford, Surrey, United Kingdom in 2015. He is currently a Ph.D. student at the University of Surrey working in the non-linear microwave measurement and modeling laboratory (n3m-labs) and specialising in multiphysics measurements of high power microwave transistors and power amplifiers. Current research aims to investigate a detailed multiphysics-based device behaviour employing conventional microwave measurement techniques in conjunction with electro-optic and thermoreflectance measurements.

Kevin Kim received the BSEE degree in Electrical Engineering from the University of Illinois at Urbana-Champaign, United States in 1994, the MSEE degree in Electrical Engineering from the University of Massachusetts at Amherst, United States in 2002, and the Ph.D. degree in Electrical Engineering from Northwestern University, Evanston, United States in 2014. He spent 16 years at Motorola Inc. in the cellular infrastructure division developing base station power amplifiers and RFIC devices. He was a RFIC design manager at Infineon Technologies before joining NXP Semiconductors in 2013 as the RF Modeling, Design Automation and Advanced RF Measurements manager where he guides the direction of NXP RF group's device modeling, EDA based design efforts and measurement technology.

Frederik Vanaverbeke received the M.A.Sc. in Electronics Engineering in 2002 from Sint Lieven Catholic College, Ghent, Belgium and the M.A.Sc. degree in Physical Engineering in 2004 from Ghent University, Belgium. Prior to joining the RF Modeling and Measurement Technology team of Freescale/NXP Semiconductors in 2012, first in Toulouse, France and later in Chandler, Arizona, USA, he has been involved in the development of Gallium Nitride technology at IMCE, VZW, in Leuven, Belgium. His interests are in harmonic load-pull measurements and in-depth characterization of Gallium-Nitride trapping effects.

Peter H. Aaen received the B.A.Sc. degree in Engineering Science and the M.A.Sc. degree in Electrical Engineering, both from the University of Toronto, Toronto, ON., Canada, and the Ph.D. degree in Electrical Engineering from Arizona State University, Tempe, AZ., USA, in 1995, 1997 and 2005, respectively. He joined the Faculty of Engineering and Physical Sciences at the University of Surrey in 2013, where he is a Reader in Microwave Semiconductor Device Modeling. He is also the Director of n3m-labs, Nonlinear Microwave Measurement and Modelling Laboratories, a joint University of Surrey / National Physical Laboratory, and the Director of NPL South of England. Before joining the University of Surrey, he was the Manager of the RF Modeling and Measurement Technology team of the RF Division of Freescale Semiconductor, Inc, Tempe, AZ, USA; a company which he joined in 1997 (then Motorola Inc. Semiconductor Product Sector). Dr. Aaen co-authored Modeling and Characterization of RF and Microwave Power FETs (Cambridge University Press, 2007).